New Journal of Physics
The open-access journal for physics

Wavenumber locking and pattern formation in spatially forced systems

Rotem Manor[1], **Aric Hagberg**[2,4] **and Ehud Meron**[1,3]

[1] Physics Department, Ben-Gurion University, Beer-Sheva 84105, Israel
[2] Theoretical Division, Los Alamos National Laboratory, Los Alamos, NM 87545, USA
[3] Institute for Dryland Environmental Research, BIDR, Ben-Gurion University, Sede Boqer Campus, 84990, Israel
E-mail: manorr@bgu.ac.il, hagberg@lanl.gov and ehud@bgu.ac.il

New Journal of Physics **11** (2009) 063016 (19pp)
Received 24 February 2009
Published 12 June 2009
Online at http://www.njp.org/
doi:10.1088/1367-2630/11/6/063016

Abstract. We study wavenumber locking and pattern formation resulting from weak spatially periodic one-dimensional forcing of two-dimensional systems. We consider systems that produce stationary or traveling stripe patterns when unforced and apply forcing aligned with the stripes. Forcing at close to twice the pattern wavenumber selects, stabilizes, or creates resonant stripes locked at half the forcing wavenumber. If the mismatch between the forcing and pattern wavenumber is high we find that the pattern still locks but develops a wave vector component perpendicular to the forcing direction and forms rectangular and oblique patterns. When the unforced system supports traveling waves, resonant rectangular patterns remain stationary but oblique patterns travel in a direction orthogonal to the traveling waves.

[4] Author to whom any correspondence should be addressed.

Contents

1. Introduction

Periodic forcing of pattern forming systems is a means of diversifying and controlling pattern formation phenomena. Forcing drives new pattern instabilities and allows control of patterns through frequency or wavenumber locking. Many types of forced systems have been studied, including spatially uniform time-periodic forcing in systems with a Hopf bifurcation [1]–[4], spatially periodic time-independent forcing of systems with finite-wavenumber instabilities [5]–[15], different cases of traveling-wave forcing [16]–[18], and multifrequency forcing [19]. Various resonances have been considered, particularly in the temporal forcing case. Resonances, $n:1$, corresponding to forcing frequencies about n times larger than the Hopf frequencies of the unforced systems, have been studied with $n=1$ [20, 21], $n=2$ [22]–[29], $n=3$ [30, 31], and $n=4$ [32]–[34].

Of these resonances, the $2:1$ temporal forcing produces a particularly rich diversity of instabilities. In addition to uniform phase instabilities of the oscillating state, which allow multiphase patterns, and the instabilities associated with the domain walls that separate different phases [2, 26], [35]–[37], the forcing also induces a primary Turing-like instability of the stationary uniform state (hereafter the 'zero state'), which coincides with the Hopf bifurcation in a Hopf–Turing codimension-two point [24, 28, 38]. This instability not only leads to richer spatiotemporal dynamics, it also extends the frequency locking range outside the locking boundaries of uniform oscillations (the $2:1$ Arnold tongue) [27].

In this paper, we consider systems that go through finite-wavenumber instabilities to periodic-stripe patterns and that are subjected to one-dimensional spatial forcing. Spatial forcing has been studied in fluid systems [5, 6, 10, 11, 15], chemical reactions [12], and in a variety of optical systems, particularly in the context of localized structures. Examples include lasers with saturable absorbers [39], photonic crystal films with Kerr nonlinearity under Fano resonance conditions [40], and a passive optical cavity containing a photonic crystal and a purely absorptive two-level medium [41].

Despite the variety of studies some basic questions related to pattern formation and wavenumber locking have not been explored. How is the wavenumber locking range of periodic-stripe patterns affected by the forcing intensity? Can the applied spatial forcing induce a primary instability of the zero state, similar to the Turing instability in the case of temporally forced

oscillatory systems? What are the implications of this instability on wavenumber locking and pattern diversity? If the unforced system supports traveling waves, how does wavenumber locking affect the traveling speed and direction?

Addressing these questions leads to some expected results, such as the widening of the stability range of stripe patterns, along with a few surprising results. Unlike the traditional view of narrow resonance tongues for weak forcing, the freedom of the system to respond in two spatial dimensions allows for a *wide* resonance range of order unity even for weak forcing. We also find, for the case of low-speed traveling waves, that the forcing can either induce stationary patterns, or patterns that travel in a direction *orthogonal* to the traveling direction in the unforced system.

Some of the results presented here have been briefly reported in [42].

2. The forced Swift–Hohenberg (SH) equation: two primary instabilities

To study periodic forcing and wavenumber locking we analyze universal normal-form equations near instability points of the zero state. Our results are therefore expected to apply to a wide range of physical systems. We derive the normal-form equations using the SH equation [43] modified to include spatial forcing and advection. This allows us to test the predictions of the normal-form analyses with numerical solutions of the modified SH equation. The SH equation is also directly relevant to several optical systems; it has been derived for a passive optical cavity [44, 45], for a degenerate optical parametric oscillator [46, 47], and for a degenerate optical parametric oscillator with a saturable absorber [48].

We consider the SH equation with up-down symmetry, to guarantee the destabilization of the zero state in a finite-wavenumber instability to periodic-stripe patterns. We add a term representing time-independent one-dimensional periodic forcing with wave vector $\mathbf{k_f} = k_f\hat{\mathbf{x}}$, and a term advecting the patterns in the x-direction. The specific form of the forced SH equation we study is

$$u_t = [\varepsilon + \gamma \cos(k_f x)]u - cu_x - (\nabla^2 + k_0^2)^2 u - u^3, \tag{1}$$

where $\gamma > 0$ is the forcing strength and c is the advection speed of the unforced stripe pattern. For now we focus on unforced systems that support stationary patterns and set $c = 0$. Forcing systems that support traveling patterns will be considered in section 3. We find it convenient to introduce a wavenumber detuning parameter

$$\nu = \frac{k_f}{2} - k_0, \tag{2}$$

and express the results in terms of ν rather than k_f. In the following we will consider small values of ν, implying proximity to a 2 : 1 resonance, as well as large negative values of order k_0.

In the absence of forcing ($\gamma = 0$) the zero state, $u = 0$, loses stability, as ε becomes positive, to a band of stationary periodic-stripe solutions centered at $\mathbf{k}_0 = (k_0, 0)$ (assuming the spatial periodicity is in the x-direction). The band of stable periodic-stripe solutions is limited by two secondary instabilities: the transverse zigzag instability at $k = k_0$, and the longitudinal Eckhaus instability at $k = k_0 + \sqrt{\varepsilon/3}/2k_0$ [49]. Figure 1 shows the patterns that develop as ε is increased from negative to positive values and starting with periodic perturbations about the zero state with wavenumbers slightly smaller (figure 1(a)) and slightly larger (figure 1(b)) than k_0. In both cases periodic-stripe patterns develop, but in the former case a secondary zigzag instability of the stripe solution leads to modulated stripes.

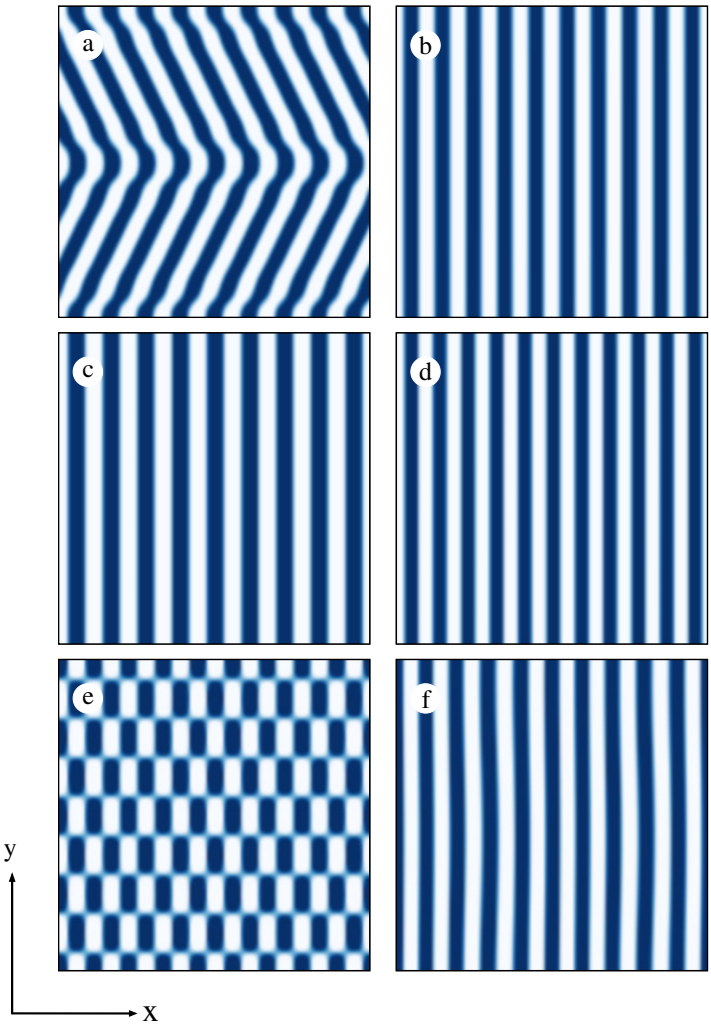

Figure 1. Patterns in the SH equation (1) with and without spatial periodic forcing. Without forcing ($\gamma = 0$) and for $\varepsilon > 0$ periodic patterns are formed with preferred wavenumber k_0. (a) For an initial condition with wavenumber slightly smaller ($k = 0.9k_0$) than k_0 a secondary zigzag instability produces modulated stripes. (b) For an initial condition with wavenumber slightly larger than k_0 ($k = 1.1k_0$) the periodic-stripe solution is in the stable band. Adding forcing, with $\gamma = 0.1$, changes the picture. (c) Starting with a resonant solution of wavenumber $k = 0.9k_0$ and $\nu = -0.1$ the forcing stabilizes the pattern and no zigzag instability is formed. (d) Starting with a resonant solution of wavenumber $k = 1.1k_0$ and $\nu = 0.1$ the resonant solution persists. (e) With random initial conditions and $\nu = -0.1$ rectangular patterns form with $k_x = 0.9k_0$ and $k_y > 0$. (f) With random initial conditions and $\nu = 0.1$ no resonant solution develops and the stripe pattern forms at the most unstable wavenumber $k_0 = 1$. Parameters: $k_0 = 1$, $\varepsilon = 0.05$, $c = 0$ and $x = y = [0, 20\pi]$.

With the presence of weak forcing ($0 < \gamma \ll 1$) in (1) the picture is different. For small detuning ($|\nu| \ll 1$) and starting with periodic perturbations about the zero state with wavenumbers that coincide with the forcing wavenumber we still get periodic-stripe solutions (figures 1(c) and (d)), except that now the forcing stabilizes the stripes at negative detuning and the zigzag instability does not develop. However, starting with *random* perturbations we get a completely different behavior; while we still get stripes in the case of positive detuning (figure 1(f)), for negative detuning *rectangular patterns* appear (figure 1(e)), suggesting the existence of a primary instability of the zero state that is induced by the forcing, and multistability ranges of one- and two-dimensional patterns.

This situation is similar to that found in periodically forced oscillatory systems where in addition to the existing Hopf bifurcation to uniform oscillations, the forcing also produces a primary instability of the zero state that breaks spatial translational symmetry. In the present case, in addition to the finite-wavenumber (stripe) instability, the forcing induces a primary instability of the zero state that breaks translational symmetry to form two-dimensional rectangular patterns.

3. Wavenumber locking of one-dimensional patterns

We first study the one-dimensional response to forcing in the form of stationary stripe solutions and address questions of stability and wavenumber locking. We assume that the forcing is weak and that the zero state of the unforced system is close to the instability threshold to stripe solutions. In the forced SH equation (1), these assumptions correspond to small values of ϵ and γ. Such solutions can be approximated by the form

$$u(x, y, t) \cong A(x, y, t)\mathrm{e}^{\mathrm{i}(k_\mathrm{f}/2)x} + \mathrm{c.c.}, \tag{3}$$

where 'c.c.' stands for the complex conjugate. Using standard multiple scale analysis [49] the following normal-form equation for the complex-valued amplitude A is obtained from (1):

$$A_t = \varepsilon A - (2\mathrm{i}k_0\partial_x - 2k_0\nu + \partial_y^2)^2 A - 3|A|^2 A + \frac{\gamma}{2}A^*, \tag{4}$$

where the star denotes the complex conjugate. This is the Newell–Whitehead–Segel equation [50, 51], generalized to include the effect of spatial periodic forcing. A similar equation has been studied in the context of defect dynamics in roll patterns [52]. We define resonant stripe patterns as stable patterns whose wave vector components in the x-direction are locked to exactly half the forcing wavenumber. Such patterns are given by solutions of (4) that are independent of x. The simplest solutions of this kind are the stationary uniform solutions

$$A_\pm = \pm\frac{1}{\sqrt{3}}\sqrt{\varepsilon - (2k_0\nu)^2 + \frac{\gamma}{2}}, \tag{5}$$

$$A_{\pm\mathrm{i}} = \pm\frac{\mathrm{i}}{\sqrt{3}}\sqrt{\varepsilon - (2k_0\nu)^2 - \frac{\gamma}{2}}. \tag{6}$$

The solutions $A_\pm$ are the first to appear as ε is increased (at $\varepsilon = -\gamma/2 + 4k_0^2\nu^2$), and are linearly stable to uniform perturbations. The solutions $A_{\pm\mathrm{i}}$ are always unstable and will not be considered further.

To find the stability of the solutions $A_\pm$ to nonuniform perturbations we use the perturbation ansatz

$$\delta A = a_+(t)\mathrm{e}^{\mathrm{i}(Q_x x+Q_y y)} + a_-(t)^*\mathrm{e}^{-\mathrm{i}(Q_x x+Q_y y)}. \tag{7}$$

Inserting (7) in (4), linearizing in $a_\pm$, and projecting onto $\exp[\mathrm{i}(Q_x x + Q_y y)]$ we obtain the linear system

$$\begin{pmatrix} \dot{a}_+ \\ \dot{a}_- \end{pmatrix} = -\begin{pmatrix} C_+ D+\gamma & D \\ D & C_+ D+\gamma \end{pmatrix}\begin{pmatrix} a_+ \\ a_- \end{pmatrix}, \tag{8}$$

where $C_\pm = (\pm 2k_0 Q_x + Q_y^2 + 2k_0\nu)^2 - (2k_0\nu)^2$ and $D = \varepsilon - (2k_0\nu)^2$. The eigenvalues of this system are

$$\sigma_\pm(Q_x, Q_y) = -D - \gamma - \frac{C_+ + C_-}{2} \pm \sqrt{D^2 + \frac{(C_+ - C_-)^2}{4}}. \tag{9}$$

The threshold for a longitudinal, or Eckhaus, instability is obtained by setting $\max(\sigma_+, \sigma_-) = 0$ with $Q_y = 0$;

$$\varepsilon_\mathrm{E} = -4k_0|\nu|\sqrt{\gamma} + 12k_0^2\nu^2, \quad |\nu| > \frac{\sqrt{\gamma}}{4k_0}. \tag{10}$$

Similarly, the threshold for a transverse, or zigzag, instability is obtained by setting $\max(\sigma_+, \sigma_-) = 0$ with $Q_x = 0$;

$$\nu_Z = -\frac{\sqrt{\gamma}}{2k_0} \quad \text{or} \quad \varepsilon_Z = 6k_0^2\nu^2 - \frac{\gamma}{2}. \tag{11}$$

Note that for $\gamma = 0$ the second zigzag threshold is always within the zigzag instability range dictated by the first threshold (except for $\nu = 0$ where they coincide) and therefore is often ignored.

The Eckhaus and zigzag instability boundaries for the unforced and forced systems are shown in figures 2(a) and (b), respectively. The shaded areas denote the range of stable stripe solutions. One obvious effect of the forcing is the extension of the stability range. Note, however, the different meaning of ν in the unforced and forced systems. In the unforced system ν is an uncontrolled quantity, selected by the system dynamics, that represents a wavenumber within the band of coexisting periodic solutions at a given ε. In the forced system ν is a control parameter of the forcing. The values of ν that correspond to stable periodic solutions for a given ε (shaded area in figure 2(b)) define the range of wavenumber locking.

Superimposing the existence and stability curves of stripe solutions of the unforced system with those of the forced system, we may distinguish among three regions, indicated by the different shades in figure 2(c), with different modes of wavenumber locking: (region I) selection of a stable solution of the unforced system with a resonant wavenumber $k_\mathrm{f}/2$, (region II) stabilization of an unstable solution of the unforced system with a resonant wavenumber, and (region III) creation of a new stable resonant solution. We have tested these modes with numerical solutions of the SH equation (1). In region I (selection), we started with random initial conditions and found resonant domains with wavenumber $k_\mathrm{f}/2$ separated by front structures. In region II (stabilization), we started with a resonant unstable solution of the unforced system, with wavenumber $k_\mathrm{f}/2$, and found a stable resonant solution with that wavenumber. In region III (creation), we started from a periodic initial condition with a wavenumber $k_\mathrm{f}/2$ and found an asymptotic resonant solution with that wavenumber.

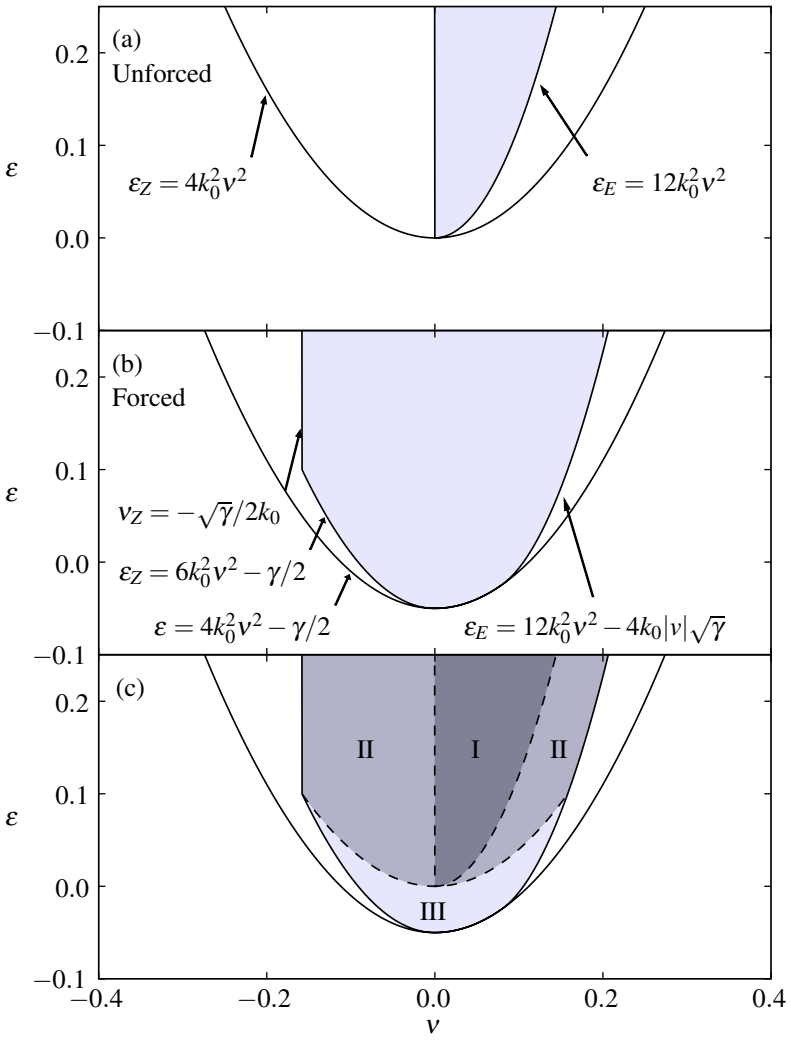

Figure 2. Existence and stability of periodic-stripe solutions of (1) for (a) the unforced ($\gamma = 0$) case and (b) the forced ($\gamma > 0$) case. The outer curves are existence boundaries while the inner curves denote the stability thresholds to Eckhaus and zigzag-type perturbations. Part (c) shows (dashed curves) the existence and stability curves of the unforced system that were displayed in part (a), superimposed on the stability domain of the forced system. These curves divide the stability domain into three different regions of wavenumber locking. Parameters: $c = 0$, $k_0 = 1$ and $\gamma = 0.1$ in (b) and (c).

It is instructive to compare these results with frequency locking in temporally forced oscillating systems. Temporally forced single oscillators share the third type of locking (wavenumber or frequency adjustments by creation of new solutions), but not the first two types, which are inherently related to the appearance of bands of modes in spatially extended system. These two locking types, however, should be found in temporally forced *spatially extended* oscillating systems. Selection and stabilization of spatial modes in this case are expected to be determined by the dispersion relation associated with the oscillatory instability.

4. Wavenumber locking of two-dimensional patterns

The effect of the forcing is not limited to modifying the existence and stability range of stripe solutions (in the x-direction). As figure 1(e) demonstrates, the forcing can also create a new mode that grows from the zero state and produces two-dimensional rectangular patterns. To study the growth of this mode and the stability properties and wavenumber locking of the resulting patterns we conduct a weakly nonlinear analysis assuming that ε and γ are small. We approximate a solution of (1) in the form

$$u \cong \tilde{a}e^{i(k_x x+k_y y)} + \tilde{b}e^{i(k_x x-k_y y)} + \text{c.c.}, \tag{12}$$

where $k_x = k_0 + \nu = k_f/2$, and $k_y = \sqrt{-2k_0\nu - \nu^2}$. With this choice $k = \sqrt{k_x^2 + k_y^2} = k_0$, the optimal wavenumber that minimizes the Lyapunov function of the SH equation. In appendix A, we derive coupled equations for the amplitudes a and b assuming they vary weakly in space and time. The equations are

$$\tilde{a}_t = \varepsilon\tilde{a} + 4(k_x\partial_x + k_y\partial_y)^2\tilde{a} + \frac{\gamma}{2}\tilde{b}^* - 3(|\tilde{a}|^2\tilde{a} + 2|\tilde{b}|^2\tilde{a}), \tag{13a}$$

$$\tilde{b}_t = \varepsilon\tilde{b} + 4(k_x\partial_x - k_y\partial_y)^2\tilde{b} + \frac{\gamma}{2}\tilde{a}^* - 3(|\tilde{b}|^2\tilde{b} + 2|\tilde{a}|^2\tilde{b}). \tag{13b}$$

Since (1) is invariant with respect to the transformation $k_f \to -k_f$ we can restrict our analysis to $k_f > 0$, or to ν values satisfying $\nu > -k_0$. Similar amplitude equations have been studied in the context of wavelength competition in convective systems [53], and in the context of time-periodic forcing of spatially extended oscillatory systems [1]. In the latter context the counterparts of rectangular and oblique pattern solutions are standing and traveling wave solutions.

Equations (13) were derived for the forced SH equation (1). In the following we will consider a more general form that can also describe other systems. Rescaling the space coordinates according to $\tilde{x} = x/4$ and $\tilde{y} = y/4$, and the amplitudes according to $a = \sqrt{3}\tilde{a}$ and $b = \sqrt{3}\tilde{b}$, we eliminate the coefficients of the spatial derivative and the uncoupled cubic terms We are still left with the (equal) coefficients of the cubic terms that couple the two modes that are specific to the SH equation, and denote them by λ. We thus consider the system

$$a_t = \varepsilon a + (k_x\partial_x + k_y\partial_y)^2 a + \frac{\gamma}{2}b^* - (|a|^2 a + \lambda|b|^2 a), \tag{14a}$$

$$b_t = \varepsilon b + (k_x\partial_x - k_y\partial_y)^2 b + \frac{\gamma}{2}a^* - (|b|^2 b + \lambda|a|^2 b), \tag{14b}$$

where for the specific case of the forced SH equation (1) $\lambda = 2$.

We first look for stationary homogeneous solutions of (14). By using the polar forms, $a = \rho_a \exp(i\alpha)$ and $b = \rho_b \exp(i\beta)$, we find the following equivalent dynamic equations for space-independent solutions:

$$\rho_{a_t} = \varepsilon\rho_a - (\rho_a^2 + \lambda\rho_b^2)\rho_a + \frac{\gamma}{2}\rho_b \cos(\varphi), \tag{15a}$$

$$\rho_{b_t} = \varepsilon\rho_b - (\rho_b^2 + \lambda\rho_a^2)\rho_b + \frac{\gamma}{2}\rho_a \cos(\varphi), \tag{15b}$$

$$\varphi_t = -\frac{\gamma}{2}\left(\frac{\rho_b}{\rho_a} + \frac{\rho_a}{\rho_b}\right)\sin(\varphi), \tag{16}$$

and

$$\psi_t = -\frac{\gamma}{2}\left(\frac{\rho_b}{\rho_a} - \frac{\rho_a}{\rho_b}\right)\sin(\varphi), \tag{17}$$

where $\varphi = \alpha + \beta$ and $\psi = \alpha - \beta$. Note first that the four-dimensional dynamics can be reduced to three dimensions; ψ is determined once ρ_a, ρ_b and φ are known. Besides the trivial solution $\rho_a = \rho_b = 0$, that corresponds to the zero state $u = 0$ of (1), equations (15) and (16) admit constant solutions of the form $\rho_a = \rho_{a0}$, $\rho_b = \rho_{b0}$, $\varphi = n\pi$, $n = 0, 1$. Linearizing (16) around this solution we find

$$\dot{\delta\varphi} = (-1)^{n+1}\frac{\gamma}{2}\left(\frac{\rho_{b_0}}{\rho_{a_0}} + \frac{\rho_{a_0}}{\rho_{b_0}}\right)\delta\varphi. \tag{18}$$

Since γ, ρ_a and ρ_b are non-negative any constant solution with $n = 1$ or $\varphi = \pi$ is unstable regardless of the ρ_a and ρ_b dynamics. We will therefore not consider these solutions any further. Inserting $\varphi = 0$ in (17) we find that ψ is constant, implying that the phases α and $\beta = -\alpha$ are constants independent of time. With $\varphi = 0$ in (15) we obtain the two-dimensional dynamical system

$$\rho_{a_t} = \varepsilon\rho_a - (\rho_a^2 + \lambda\rho_b^2)\rho_a + \frac{\gamma}{2}\rho_b, \tag{19a}$$

$$\rho_{b_t} = \varepsilon\rho_b - (\rho_b^2 + \lambda\rho_a^2)\rho_b + \frac{\gamma}{2}\rho_a. \tag{19b}$$

Equations (19) admit the constant solution

$$\rho_a = \rho_b = \rho_0, \tag{20}$$

where

$$\rho_0 = \sqrt{\frac{\varepsilon + \gamma/2}{1+\lambda}}. \tag{21}$$

In terms of the amplitudes a and b this form gives the one-parameter family of solutions

$$a_0 = \rho_0 \exp(\mathrm{i}\alpha), \qquad b_0 = \rho_0 \exp(-\mathrm{i}\alpha). \tag{22}$$

These solutions exist for $\varepsilon > -\gamma/2$ and $-2k_0 < \nu < 0$ (in order for k_y to be real), and describe *rectangular* patterns. The undetermined constant phase α is associated with the continuous translation symmetry in the y-direction, which is not broken by the forcing.

In addition (19) admit the constant solutions

$$\rho_a = \rho_\pm, \quad \rho_b = \rho_\mp, \tag{23}$$

where

$$\rho_\pm = \sqrt{\frac{\varepsilon \pm \sqrt{\varepsilon^2 - \frac{\gamma^2}{(\lambda-1)^2}}}{2}}. \tag{24}$$

In terms of the amplitudes a and b this form gives the one-parameter family of solutions

$$a_\pm = \rho_\pm \exp(\mathrm{i}\alpha), \tag{25a}$$

$$b_\mp = \rho_\mp \exp(-\mathrm{i}\alpha), \tag{25b}$$

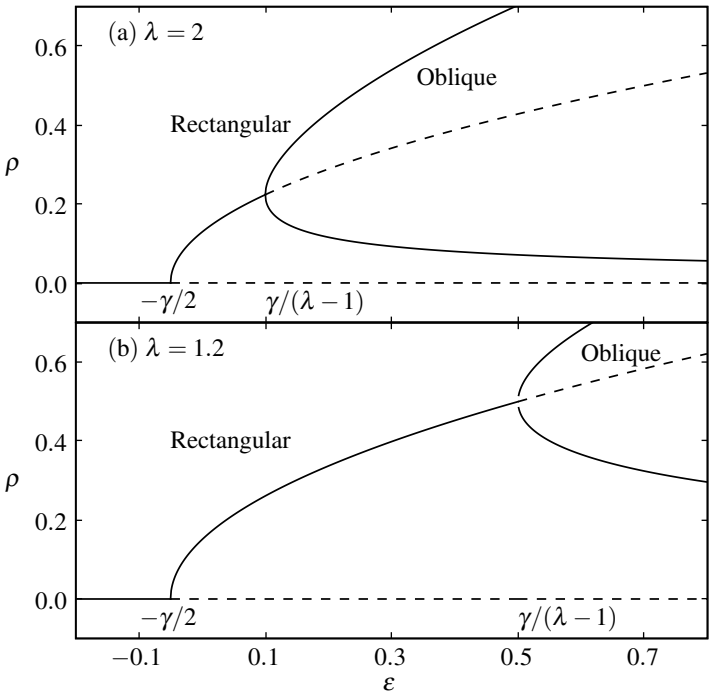

Figure 3. Bifurcation diagrams for solutions of the amplitude equations (15) for (a) $\lambda = 2$, the value obtained for the forced SH equation, and (b) $\lambda = 1.2$ ($\gamma = 0.1$). Rectangular patterns (ρ_0) appear at $\varepsilon = -\gamma/2$ (see (21)), and become unstable to oblique patterns ($\rho_\pm$) at $\varepsilon = \gamma/(\lambda - 1)$ (see (24)). Values of λ closer to 1 shift the instability of rectangular patterns to higher ε values.

where α is again an arbitrary constant. These solutions exist for $\varepsilon > \gamma/(\lambda - 1)$ and $-2k_0 < \nu < 0$. They break the symmetry, $a \to b$, $b \to a$, of (15), and describe *oblique* patterns.

We now examine the linear stability of these solutions to uniform perturbations. We have also studied the stability to nonuniform perturbations and found that the stability ranges coincide with those for uniform perturbations [54]. Linearizing (19) around a constant solution $\rho_a = \rho_{a_0}$, $\rho_b = \rho_{b_0}$, and solving for the eigenvalues we find

$$\sigma_\pm = \varepsilon - \frac{3+\lambda}{2}\left(\rho_{a_0}^2 + \rho_{b_0}^2\right) \pm \sqrt{\frac{(3-\lambda)^2}{4}\left(\rho_{a_0}^2 - \rho_{b_0}^2\right)^2 + \left(\frac{\gamma}{2} - 2\lambda\rho_{b_0}\rho_{a_0}\right)^2}. \tag{26}$$

The stability of the zero state ($a = b = 0$) can be calculated directly from (14); it is stable for $\varepsilon < -\gamma/2$. The stability of rectangular and oblique patterns is inferred from (26). For rectangular patterns, given by (22), we find the stability range $-\gamma/2 < \varepsilon < \gamma/(\lambda - 1)$. For oblique patterns, given by (25), we find the stability range $\varepsilon > \gamma/(\lambda - 1)$. These results are summarized in the bifurcation diagram shown in figure 3.

The solutions representing the rectangular patterns and the oblique patterns are constant, which implies that both are locked at half the forcing wavenumber, $k_x = k_f/2$. Unlike the wavenumber locking of stripe patterns, which is restricted to a detuning range that scales with the forcing strength and therefore is very narrow for weak forcing, rectangular and oblique patterns are resonant over a wide and continuous detuning range, $|\nu| \sim O(1)$, even for diminishingly small forcing intensities γ. This wide locking range results from the

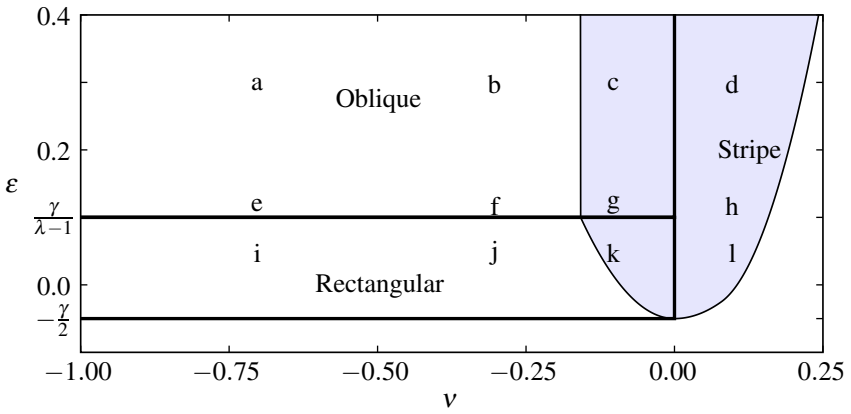

Figure 4. Phase diagram in the ν–ε parameter plane showing the regions of stable resonant patterns. The resonance range of stable $2:1$ stripe patterns (shaded region) is much narrower ($|\nu| \sim O(\sqrt{\varepsilon})$) than the resonance ranges of rectangular and oblique patterns ($|\nu| \sim O(1)$). Stripes and rectangular or oblique patterns coexist for $\nu < 0$ and within the stripe stability region. The horizontal boundaries for the stability of rectangular and oblique patterns are found from (26). Parameters: $k_0 = 1$, $\gamma = 0.1$ and $\lambda = 2$.

freedom of the system to build a wave vector component in the y-direction while keeping the x-component locked to half of the forcing wavenumber $k_x = k_f/2$. This result could be significant for applications where periodic forcing is used as a means of controlling the wavenumber of a pattern; adding a second spatial dimension will dramatically increase the range over which the wavenumber can be controlled. Figure 4 shows the boundaries of stable $2:1$ wavenumber-locked stripe solutions along with the parameter ranges for rectangular and oblique patterns.

5. Wavenumber locking of traveling patterns

To what extent are the results found in the previous section valid for the case where the unforced system supports traveling waves rather than stationary patterns? Are wavenumber-locked patterns stationary or traveling, and if they travel, in what direction? To address these questions we consider a system with one-dimensional traveling wave solutions in the x-direction (when unforced) with spatially periodic forcing also in the x-direction. The amplitude equations for this case are

$$a_t = (\varepsilon - \mathrm{i}\omega)a + (k_x\partial_x + k_y\partial_y)^2 a + \frac{\gamma}{2}b^* - (|a|^2 a + \lambda|b|^2 a), \tag{27a}$$

$$b_t = (\varepsilon - \mathrm{i}\omega)b + (k_x\partial_x - k_y\partial_y)^2 b + \frac{\gamma}{2}a^* - (|b|^2 b + \lambda|a|^2 b), \tag{27b}$$

where $\omega = ck_x$ and c is the traveling-wave speed of the unforced pattern which we assume to be small (of order ε). These equations, with $\lambda = 2$ can be derived from (1) with $c \neq 0$.

Expressing the amplitudes in polar form as before, $a = \rho_a \exp(\mathrm{i}\alpha)$ and $b = \rho_b \exp(\mathrm{i}\beta)$, we find that the equations for the moduli ρ_a and ρ_b and for the phase difference $\psi = \alpha - \beta$ remain

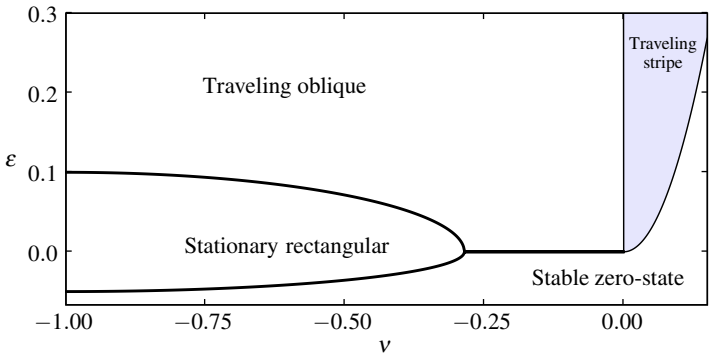

Figure 5. Phase diagram for weakly forced systems supporting traveling stripes. In contrast to the $c = 0$ case of the forced SH model (1) (figure 4), when $c \neq 0$ the stationary rectangular patterns occupy a smaller region, the oblique patterns travel and occupy a larger region, and the zero-state can lose stability directly to oblique patterns. When the forcing is sufficiently weak, the stripe patterns travel and occupy the same region as the stationary stripe patterns do in the unforced system. Parameters: $k_0 = 1$, $\gamma = 0.1$ and $c = 0.07$.

unchanged but the equation for the phase variable $\varphi = \alpha + \beta$ is now

$$\varphi_t = -2\omega - \frac{\gamma}{2}\left(\frac{\rho_b}{\rho_a} + \frac{\rho_a}{\rho_b}\right)\sin(\varphi). \tag{28}$$

Looking for stationary solutions of (28) we find

$$\sin\varphi = -\frac{ck_\mathrm{f}}{\gamma R}, \qquad R = \frac{1}{2}\left(\frac{\rho_b}{\rho_a} + \frac{\rho_a}{\rho_b}\right). \tag{29}$$

Of the two solutions for φ only

$$\varphi_0 = -\arcsin(ck_\mathrm{f}/\gamma R), \tag{30}$$

is stable (see earlier discussion). Defining an effective forcing strength

$$\tilde{\gamma} = \gamma\cos\,\varphi_0 = \sqrt{\gamma^2 - \frac{c^2k_\mathrm{f}^2}{R^2}}, \tag{31}$$

the equations for ρ_a and ρ_b become identical to (19) with γ replaced by $\tilde{\gamma}$. Rectangular patterns then appear at $\varepsilon = -\tilde{\gamma}/2$ and lose stability to oblique patterns at $\varepsilon = \tilde{\gamma}/(\lambda - 1)$. Note that for rectangular patterns $\psi_t = 0$, despite the fact that $\sin(\varphi) \neq 0$, because $\rho_a = \rho_b$. Since constant ψ implies that the phases α and β are constant as well, the rectangular patterns are stationary and wavenumber locked. Figure 5 shows the regime of stable rectangular patterns. For larger traveling-wave velocity c the regime of locked rectangular patterns is smaller.

Oblique patterns appear when $\varepsilon > \tilde{\gamma}/(\lambda - 1)$. These patterns are no longer stationary because $\rho_a \neq \rho_b$ and $\psi_t \neq 0$. They do not travel in the x-direction, as the traveling waves in the unforced system do, but instead in the *orthogonal direction* y, the direction along which the continuous translational symmetry is not broken by the forcing. To obtain this result we first insert the stationary solution (30) of (28) into the equation for ψ

$$\psi_t = \frac{\gamma}{2}\left(\frac{\rho_b}{\rho_a} - \frac{\rho_a}{\rho_b}\right)\frac{ck_\mathrm{f}}{\gamma R} \equiv \Omega. \tag{32}$$

Since Ω is constant $\psi(t) = \Omega t + \psi_0$ where ψ_0 is an integration constant. The phases α and β are then

$$\alpha = \frac{\Omega t}{2} + \alpha_0, \qquad \beta = -\frac{\Omega t}{2} + \beta_0, \tag{33}$$

where $\alpha_0 = (\varphi_0 + \psi_0)/2$, and $\beta_0 = (\varphi_0 - \psi_0)/2$, and the solution form (12) becomes

$$u \propto \rho_a e^{i\alpha_0} e^{ik_x x + ik_y(y+vt)} + \rho_b e^{i\beta_0} e^{ik_x x - ik_y(y+vt)} + \text{c.c.}, \tag{34}$$

where $v = \Omega/(2k_y)$. This form describes an oblique pattern traveling in the y-direction with a wave vector component in the x-direction locked to half the forcing wavenumber, $k_x = k_f/2$. Since the two symmetric oblique patterns have opposite signs of Ω they propagate in opposite directions. The region of stable traveling oblique patterns is shown in figure 5. Note that the oblique patterns may form directly from the zero state if c is large enough.

When the detuning ν is positive the two-dimensional resonant patterns cease to exist but stripe patterns may exist as they do for the case $c = 0$ where the unforced system supports stationary patterns. These patterns are described by an amplitude equation similar to (4) but with an additional term $-ick_0$ on the right-hand side. A linear stability analysis of the zero state $A = 0$ gives the stability boundary $\varepsilon = 4k_0^2\nu^2$ for sufficiently weak forcing, $\gamma < 2|c|k_0$. Above this threshold, which coincides with that of the unforced system, traveling stripes appear. The existence range of these patterns for positive detuning is described by the shaded area in figure 5. For small negative detuning these patterns coexist with resonant two-dimensional patterns. Direct numerical studies of the forced traveling SH equation support these results but also indicate the possible coexistence of unlocked traveling oblique patterns whose wave velocity has a nonzero component in the x-direction, unlike the locked traveling oblique patterns.

6. Pattern diversity

The leading-order solution form (12), where the amplitudes a and b represent rectangular patterns (22) and oblique patterns (25), can be used to map the two-dimensional patterns in the ε–ν plane. As figure 6 shows, both rectangular and oblique patterns change from stripe patterns along the x-direction, in the limit $\nu \to 0$, to stripe patterns along the y-direction, in the limit $\nu \to -k_0$. Accordingly, the pattern's wave vector component in the x-direction is continuously controllable by the forcing from $k_x = k_0$ ($\nu = 0$) to $k_x = 0$ ($\nu = -k_0$). At $\nu = -k_0/4$ the rectangular patterns are square and the oblique stripes are exactly diagonal. In the range $\varepsilon \gg \gamma/(\lambda - 1)$, the oblique patterns become oblique stripes. Direct numerical solutions of the forced SH equation (1) confirm these results as figure 7 shows.

The pattern boundaries in figure 4 indicate a bistability range of stripes and rectangular patterns for $\varepsilon < \gamma/(\lambda - 1)$, and a tristability range of stripes with the two symmetric oblique patterns for $\varepsilon > \gamma/(\lambda - 1)$. These multistability ranges allow for asymptotic spatial mixtures of different patterns [42]. For $\varepsilon < \gamma/(\lambda - 1)$ asymptotic spatial mixtures of stripe and rectangular patterns are found whenever the domain walls that separate the two patterns are perpendicular to the stripe direction. Such domain walls are close approximations of stationary transverse Ising fronts [52]. Domain walls aligned parallel to the stripes propagate to reduce and eliminate stripe domains, leaving an asymptotic rectangular pattern. Fronts may also form between stripes and oblique patterns but in that case the fronts may be either aligned perpendicular or parallel to the stripes.

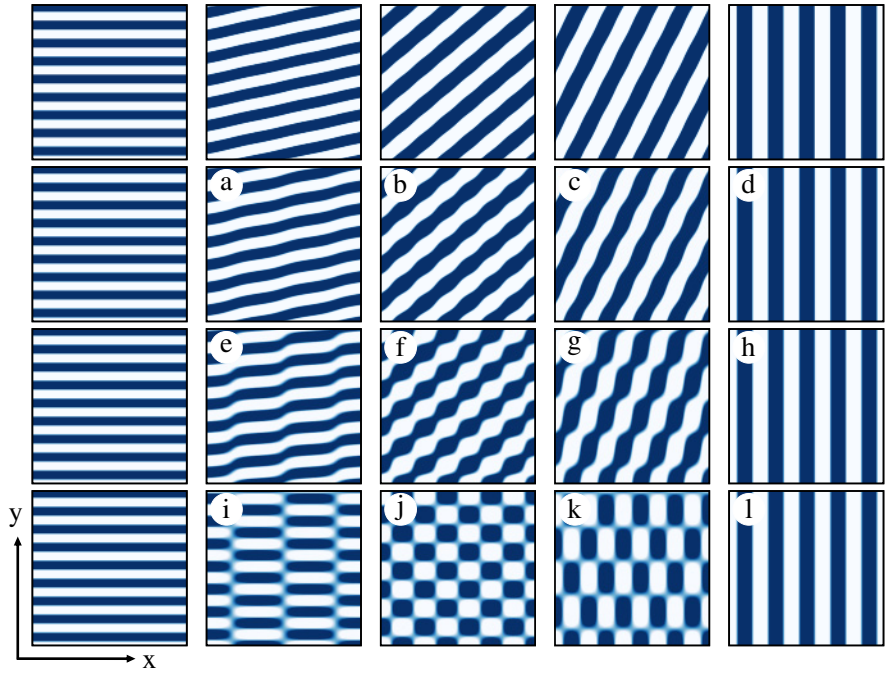

Figure 6. Solutions of the leading order approximation (12) show the diversity of patterns. As ν is varied from $-k_0 \to 0$ (left to right) the pattern changes from horizontal stripes, to squares or oblique patterns, and then to vertical stripes through a continuous variation in k_x from 0 to k_0. The patterns in (a)–(l) correspond to the parameters at the points specified in figure 4. Parameters: $c = 0,\ \lambda = 2,\ k_0 = 1,\ \alpha = 0,\ \gamma = 0.1,\ \nu = [-1.0, -0.777, -0.2, -0.05, 0.1]$, $\varepsilon = [0.05, 0.12, 0.3, 1]$ and $x = y = [0, 10\pi]$.

When the unforced system supports traveling waves, the two symmetric oblique patterns in the forced system travel in opposite directions along the y-axis. This suggests the possible existence of sink and source solutions that separate domains of incoming traveling waves or outgoing traveling waves. Such solutions of (1) (with $c > 0$) indeed exist as figure 8 shows.

We restricted the discussion of wavenumber locking of one-dimensional stripe patterns to the 2 : 1 resonance, where $k_f \approx 2k_0$, and found that the locking range overlaps with that of two-dimensional patterns. By decreasing the forcing wavenumber k_f from $2k_0$ to k_0 other resonances of stripe patterns, such as 3 : 2 and 1 : 1, may be encountered. Overlapping regions of these stripe patterns with the resonance range of two-dimensional patterns, can give rise to additional types of spatially mixed patterns.

7. Conclusion

One-dimensional spatial periodic forcing of two-dimensional pattern forming systems can strongly effect pattern formation. Forcing close to an exact 2 : 1 resonance can stabilize resonant stripe patterns and even extend their existence range. However, when the forcing wavenumber is too small (relative to $2k_0$) two-dimensional rectangular patterns appear from the zero state, which further destabilize to a pair of oblique patterns. These two-dimensional patterns are

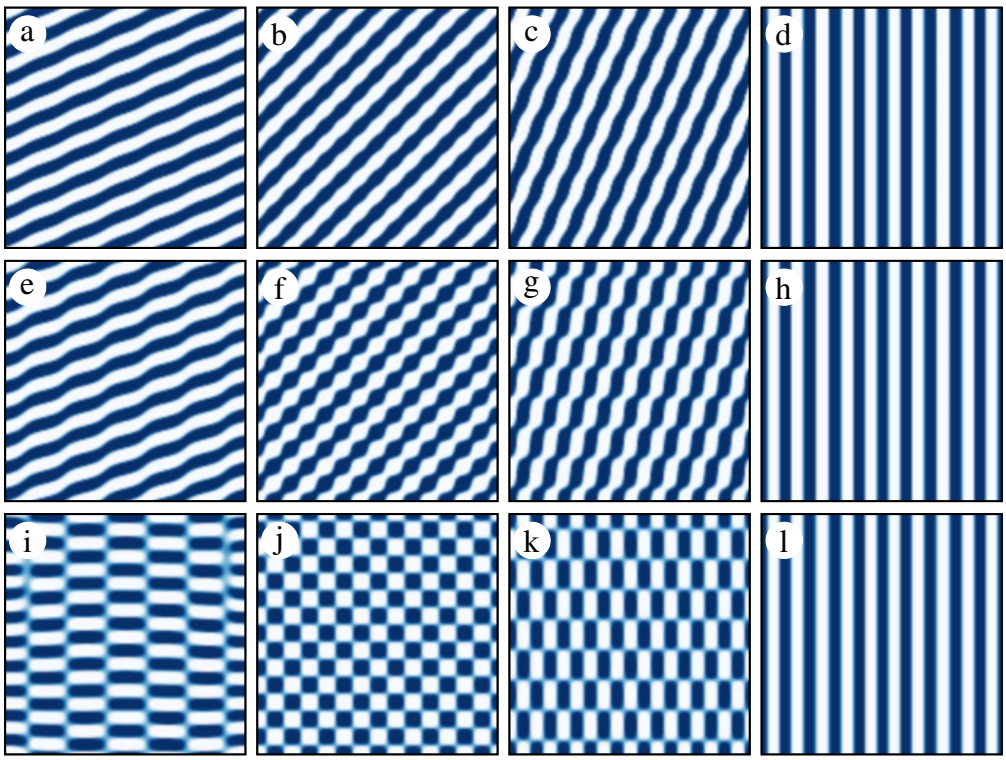

Figure 7. Numerical solutions of stationary resonant patterns in (1) obtained by varying the forcing wavenumber ν and driving ε. The pattern forms exactly match those of the amplitude equations for the same parameters. The patterns in (a)–(l) correspond to the parameters at the points specified in figure 4. Patterns (c), (g) and (k) coexist with stable stripe patterns (not shown) at the same parameters. Parameters: $c = 0$, $k_0 = 1$, $\gamma = 0.1$, $\nu = [-0.7, -0.3, -0.1, 0.1]$, $\varepsilon = [0.05, 0.12, 0.3]$ and $x = y = [0, 20\pi]$.

resonant in the sense that their wave vector components in the forcing direction are exactly half the forcing wavenumber. To compensate for the total wavenumber they develop wave vector components in the orthogonal direction. When the unforced system supports traveling stripes, rather than stationary stripes, resonant rectangular and oblique patterns still appear. However, while the rectangular patterns are stationary and occupy a smaller domain in the (ε, ν) parameter plane relative to the stationary-stripe case, oblique patterns travel and occupy a larger domain in this parameter plane. Surprisingly, the direction of travel for oblique patterns is orthogonal to the direction of stripe patterns in the unforced system.

The results predicted in this study can be tested in controlled experiments. Two candidate systems are Rayleigh–Bénard convection forced by modulating the shape of the bottom plate [14], and the light-sensitive CDIMA chemical reaction forced by masked illumination of the reaction cell [12]. A possible environmental application of this study is the restoration of banded vegetation in arid and semi-arid regions. Vegetation on hill slopes often self-organizes to form stripe patterns oriented perpendicular to the slope direction [55, 56], which slowly migrate uphill. A common restoration practice of degraded vegetation is based on water harvesting by means of parallel contour ditches that accumulate runoff and along which the vegetation is

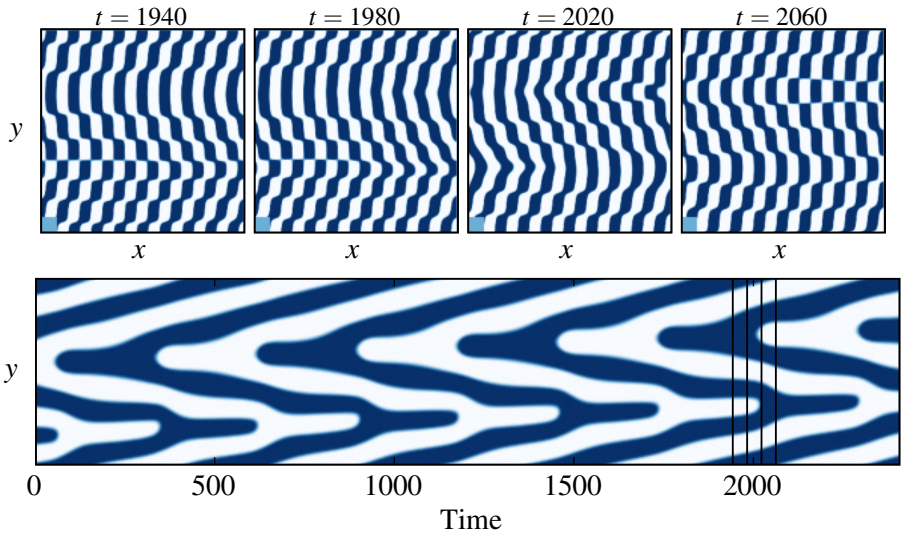

Figure 8. Counterpropagating oblique waves in the forced SH equation (1) with $c > 0$. (top) Four frames at different times show the pattern dynamics. The waves in the center propagate downward and the waves near the top and bottom propagate upward producing a corresponding wave sink and wave source. (bottom) A space–time plot of the same data for a slice along the y direction in the center of the pattern above. The source near the top of the domain and the sink near the bottom are clearly visible. The vertical lines correspond to the time of the pattern images in the frames above. Parameters: $c = 0.5$, $k_0 = 1$, $\gamma = 0.1$, $\nu = -0.1$, $\varepsilon = 0.05$ and $x = y = [0, 20\pi]$.

planted. The contour ditches, which increase the biomass growth rate because of the higher soil-water content they induce [57, 58], can be regarded as multiplicative periodic forcing as modeled in (1).

Acknowledgments

We thank Mustapha Tlidi for helpful suggestions in preparing this manuscript. The support of the James S McDonnell Foundation is gratefully acknowledged. Part of this work was funded by the Department of Energy at Los Alamos National Laboratory under contract DE-AC52-06NA25396, and the DOE Office of Science Advanced Computing Research (ASCR) program in Applied Mathematical Sciences.

Appendix A. Amplitude equations for two-dimensional patterns

We consider (1), assuming $\varepsilon \ll 1$ and $\gamma := \varepsilon\Gamma$ with $\Gamma \sim O(1)$. Expanding the solution u as

$$u = \varepsilon^{1/2}u_1 + \varepsilon u_2 + \varepsilon^{3/2}u_3 + \cdots, \tag{A.1}$$

and rescaling time and space as

$$X = \varepsilon^{1/2}x, \quad Y = \varepsilon^{1/2}y, \quad T = \varepsilon t, \tag{A.2}$$

we find at order $\varepsilon^{1/2}$

$$(\partial_x^2+\partial_y^2+k_0^2)^2 u_1 = 0. \tag{A.3}$$

To describe rectangular patterns we consider a solution of this equation in the form

$$u_1 = \tilde{a}(X,Y,T)\mathrm{e}^{\mathrm{i}(k_x x+k_y y)} + \tilde{b}(X,Y,T)\mathrm{e}^{\mathrm{i}(k_x x-k_y y)} + \text{c.c.}, \tag{A.4}$$

where $k_x = k_0+\nu$ and $k_y = \sqrt{-2k_0\nu-\nu^2}$. At order ε we find that u_2 satisfies the same equation as u_1, and choose the solution $u_2 = 0$. At order $\varepsilon^{3/2}$ we obtain

$$(\partial_x^2+\partial_y^2+k_0^2)^2 u_3 = -\frac{\partial u_1}{\partial T} + u_1 - u_1^3 - 4(\partial_x\partial_X+\partial_y\partial_Y)^2 u_1 + \Gamma u_1\cos[2(k_0+\nu)x]. \tag{A.5}$$

Substituting (A.4) into (A.5), we obtain

$$(\partial_x^2+\partial_y^2+k_0^2)^2 u_3 = \alpha_+\mathrm{e}^{\mathrm{i}k_x x+\mathrm{i}k_y y} + \alpha_-\mathrm{e}^{\mathrm{i}k_x x-\mathrm{i}k_y y} + \text{c.c.} + \text{nonresonant terms}, \tag{A.6}$$

where

$$\alpha_+ = \tilde{a}_T - \tilde{a} + 3(|\tilde{a}|^2\tilde{a}+2|\tilde{b}|^2\tilde{a}) - 4(k_x\partial_X+k_y\partial_Y)^2\tilde{a} - \frac{\Gamma}{2}\tilde{b}^* \tag{A.7a}$$

$$\alpha_- = \tilde{b}_T - \tilde{b} + 3(|\tilde{b}|^2\tilde{b}+2|\tilde{a}|^2\tilde{b}) - 4(k_x\partial_X-k_y\partial_Y)^2\tilde{b} - \frac{\Gamma}{2}\tilde{a}^*. \tag{A.7b}$$

Solvability of (A.6) requires the elimination of the resonant terms $\exp(\mathrm{i}k_x x \pm \mathrm{i}k_y y)$ from the right-hand side. Setting the coefficients of these terms to zero ($\alpha_\pm = 0$), going back to the original space and time variables (x, y, t), and denoting $a = \sqrt{\varepsilon}\tilde{a}$, $b = \sqrt{\varepsilon}\tilde{b}$ we obtain (13).

References

[1] Riecke H, Crawford J D and Knobloch E 1988 Time-modulated oscillatory convection *Phys. Rev. Lett.* **61** 1942–5

[2] Coullet P, Lega J, Houchmanzadeh B and Lajzerowicz J 1990 Breaking chirality in nonequilibrium systems *Phys. Rev. Lett.* **65** 1352

[3] Lin A L, Bertram M, Martinez K, Swinney H L, Ardelea A and Carey G F 2000 Resonant phase patterns in a reaction–diffusion system *Phys. Rev. Lett.* **84** 4240–3

[4] Lin A L, Hagberg A, Meron E and Swinney H L 2004 Resonance tongues and patterns in periodically forced reaction–diffusion systems *Phys. Rev.* E **69** 066217

[5] Kelly R E and Pal D 1978 Thermal convection with spatially periodic boundary conditions resonant wavelength excitation *J. Fluid Mech.* **86** 433–56

[6] Lowe M, Gollub J P and Lubensky T C 1983 Commensurate and incommensurate structures in a nonequilibrium system *Phys. Rev. Lett.* **51** 786–9

[7] Coullet P 1986 Commensurate–incommensurate transition in nonequilibrium systems *Phys. Rev. Lett.* **56** 724–7

[8] Coullet P and Huerre P 1986 Resonance and phase solitons in spatially-forced thermal convection *Physica* D **23** 27–44

[9] Curado E M F and Elphick C 1987 Effects of an almost resonant spatial thermal modulation in the Rayleigh–Benard problem: quasiperiodic behaviour *J. Phys. A: Math. Gen.* **20** 1205–14

[10] Pismen L M 1987 Bifurcation of quasiperiodic and nonstationary patterns under external forcing *Phys. Rev. Lett.* **59** 2740–3

[11] Schmitz R and Zimmermann R W 1996 Spatially periodic modulated Rayleigh–Bénard convection *Phys. Rev.* E **53** 5993–6011

[12] Dolnik M, Berenstein I, Zhabotinsky A M and Epstein I R 2001 Spatial periodic forcing of Turing structures *Phys. Rev. Lett.* **87** 238301
[13] Peter R, Hilt M, Ziebert F, Bammert J, Erlenkämper C, Lorscheid N, Weitenberg C, Winter A, Hammele M and Zimmermann W 2005 Stripe-hexagon competition in forced pattern-forming systems with broken up-down symmetry *Phys. Rev.* E **71** 046212
[14] McCoy J 2007 Adventures in pattern formation: spatially periodic forcing and self-organization *PhD Thesis* Cornell University
[15] Seiden G, Weiss S, McCoy J H, Pesch W and Bodenschatz E 2008 Pattern forming system in the presence of different symmetry-breaking mechanisms *Phys. Rev. Lett.* **101** 214503
[16] Míguez D G, Nicola E M, Muñuzuri A P, Casademunt J, Sagués F and Kramer L 2004 Traveling-stripe forcing generates hexagonal patterns *Phys. Rev. Lett.* **93** 048303
[17] Rüdiger S, Nicola E M, Casademunt J and Kramer L 2007 Theory of pattern forming systems under traveling-wave forcing *Phys. Rep.* **447** 73–1111
[18] Beetz A, Gollwitzer C, Richter R and Rehberg I 2008 Response of a ferrofluid to traveling-stripe forcing *J. Phys.: Condens. Matter* **20** 204109
[19] Conway J M and Riecke H 2007 Quasipatterns in a model for chemical oscillations forced at multiple resonance frequencies *Phys. Rev. Lett.* **99** 218301
[20] Chaté H, Pikovsky A and Rudzick O 1999 Forcing oscillatory media: phase kinks vs. synchronization *Physica* D **131** 17–30
[21] Park H-K 2001 Frequency locking in spatially extended systems *Phys. Rev. Lett.* **86** 1130–3
[22] Coullet P and Emilsson K 1992 Strong resonances of spatially distrubuted oscillatiors: a laboratory to study patterns and defects *Physica* D **61** 119–31
[23] Petrov V, Ouyang Q and Swinney H L 1997 Resonant pattern formation in a chemical system *Nature* **388** 655–7
[24] Yochelis A, Hagberg A, Meron E, Lin A L and Swinney H L 2002 Development of standing-wave labyrinthine patterns *SIAM J. Appl. Dyn. Sys.* **1** 236–47
[25] Marts B, Martinez K and Lin A L 2004 Front dynamics in an oscillatory bistable Belousov–Zhabotinsky chemical reaction *Phys. Rev.* E **70** 056223
[26] Marts B, Hagberg A, Meron E and Lin A L 2004 Bloch-front turbulence in a periodically forced Belousov–Zhabotinsky reaction *Phys. Rev. Lett.* **93** 108305
[27] Yochelis A, Elphick C, Hagberg A and Meron E 2004 Two-phase resonant patterns in forced oscillatory systems *Physica* D **199** 201–22
[28] Yochelis A, Elphick C, Hagberg A and Meron E 2005 Frequency locking in extended systems: the impact of a Turing mode *Europhys. Lett.* **69** 170–6
[29] Yochelis A, Burke J and Knobloch E 2006 Reciprocal oscillons and nonmonotonic fronts in forced nonequilibrium systems *Phys. Rev. Lett.* **97** 254501
[30] Gallego R, Walgraef D, San Miguel M and Toral R 2001 Transition from oscillatory to excitable regime in a system forced at three times its natural frequency *Phys. Rev.* E **64** 056218
[31] Hemming C and Kapral R 2002 Front explosion in a resonantly forced complex Ginzburg–Landau system *Physica* D **168** 10–22
[32] Elphick C, Hagberg A and Meron E 1998 A phase front instability in periodically forced oscillatory systems *Phys. Rev. Lett.* **80** 5007–10
[33] Elphick C, Hagberg A and Meron E 1999 Multiphase patterns in periodically forced oscillatory systems *Phys. Rev.* E **59** 5285–91
[34] Lin A L, Hagberg A, Ardelea A, Bertram M, Swinney H L and Meron E 2000 Four-phase patterns in forced oscillatory systems *Phys. Rev.* E **62** 3790–8
[35] Esteban-Martín A, Taranenko V B, García J, de Valcárcel G J and Roldán E 2005 Controlled observation of a nonequilibrium Ising–Bloch transition in a nonlinear optical cavity *Phys. Rev. Lett.* **94** 223903
[36] Sánchez-Morcillo V J, Espinosa V, Pérez-Arjona I, Silva F, de Valcárcel G J and Roldán E 2005 Domain wall dynamics in an optical Kerr cavity *Phys. Rev.* E **71** 066209

[37] Taranenko V B, Esteban-Martín A, de Valcárcel G J and Roldán E 2006 Hysteretic nonequilibrium Ising–Bloch transition *Phys. Rev.* E **73** 027201
[38] Coullet P, Frisch T and Sonnino G 1994 Dispersion-induced patterns *Phys. Rev.* E **49** 2087–90
[39] Staliunas K 2003 Midband dissipative spatial solitons *Phys. Rev. Lett.* **91** 053901
[40] Yulin A, Skryabin D and Russell P 2005 Dissipative localized structures of light in photonic crystal films *Opt. Express* **13** 3529–34
[41] Vladimirov A G, Skryabin D V, Kozyreff G, Mandel P and Tlidi M 2006 Bragg localized structures in a passive cavity with transverse modulation of the refractive index and the pump *Opt. Express* **14** 1–6
[42] Manor R, Hagberg A and Meron E 2008 Wave-number locking in spatially forced pattern-forming systems *Europhys. Lett.* **83** 10005
[43] Swift J and Hohenberg P C 1977 Hydrodynamic fluctuations at the convective instability *Phys. Rev.* A **15** 319–28
[44] Mandel P, Georgiou M and Erneux T 1993 Transverse effects in coherently driven nonlinear cavities *Phys. Rev.* A **47** 4277–86
[45] Tlidi M, Georgiou M and Mandel P 1993 Transverse patterns in nascent optical bistability *Phys. Rev.* A **48** 4605–9
[46] Longhi S and Geraci A 1996 Swift–Hohenberg equation for optical parametric oscillators *Phys. Rev.* A **54** 4581–4
[47] Musslimani A H 1998 Long-wave instability in optical parametric oscillators *Physica* A **249** 141–5
[48] Tlidi M and Taki M 2003 Increasing spatial complexity toward near-resonant regimes of quadratic media *Phys. Rev. Lett.* **91** 023901
[49] Cross M C and Hohenberg P C 1993 Pattern formation outside of equilibrium *Rev. Mod. Phys.* **65** 851
[50] Newell A C and Whitehead J A 1969 Finite bandwidth, finite amplitude convection *J. Fluid Mech.* **38** 279
[51] Segel L A 1969 Distant side-walls cause slow amplitude modulation of cellular convection *J. Fluid Mech.* **38** 203
[52] Korzinov L L, Rabinovich M I and Tsimring L S 1992 Symmetry breaking in nonequilibrium systems: interaction of defects *Phys. Rev.* A **46** 7601–7
[53] Zimmermann W, Ogawa A, Kai S, Kawasaki K and Kawakatsu T 1993 Wavelength competition in convective systems *Europhys. Lett.* **24** 217–22
[54] Manor R 2006 Pattern formation in spatially forced systems *Master's Thesis* Ben–Gurion University of the Negev
[55] Valentin C, d'Herbès J M and Poesen J 1999 Soil and water components of banded vegetation patterns *Catena* **37** 1–24
[56] Yizhaq H, Gilad E and Meron E 2005 Banded vegetation: biological productivity and resilience *Physica* A **356** 139–44
[57] von Hardenberg J, Meron E, Shachak M and Zarmi Y 2001 Diversity of vegetation patterns and desertification *Phys. Rev. Lett.* **87** 198101
[58] Gilad E, von Hardenberg J, Provenzale A, Shachak M and Meron E 2004 Ecosystem engineers: from pattern formation to habitat creation *Phys. Rev. Lett.* **93** 098105